

Recent Developments in Standing-Wave Oscillator Design: Review

(Invited Paper)

William Andress and Donhee Ham

Harvard University, Cambridge, MA 02138, USA

Abstract— This paper summarizes the most recent advances in wave-based oscillator design, reviewing various manifestations of the traveling wave oscillator and the standing wave oscillator. We then review and analyze our latest development of standing wave oscillator design utilizing wave-adaptive tapered transmission lines, which is originally reported in [1]. This structure lowers phase noise through loss-reducing shaping of the transmission line, such that it is adapted to the position-dependent standing wave amplitudes. Demonstrating the benefits of standing-wave-based operations, this novel design concept boosts the potential for the emergence of standing wave oscillators as a useful alternative to the traditional LC oscillator.

Index Terms— oscillators, traveling wave oscillators, standing wave oscillators, tapered transmission lines, phase noise, radio-frequency.

1. INTRODUCTION

While a prevalent class of RF oscillators relies on lumped LC resonators, an oscillator type that operates instead upon wave behaviors has recently emerged. Sections 2 and 3 of this paper review these wave-based oscillators, categorized into traveling wave oscillators (TWO) [2] - [4] and standing wave oscillators (SWO) [5] - [7].

Wave-based oscillators strongly fulfill certain design criteria, including high-frequency operation [2] [3] and low-skew low-jitter clock distribution [6]. But as of yet, the advantages of wave behaviors in terms of resonator Q and oscillator phase noise have not been readily apparent. The authors have recently demonstrated in [1] that standing wave oscillators (SWO) are indeed well-suited to a valuable exploitation of wave properties that enhances resonator Q and lowers phase noise. Standing waves are unique in that the current and voltage amplitudes vary with position. The transmission line loss characteristics can be adapted to these amplitude variations through *tapering* to reduce loss and improve phase noise significantly. This work is originally treated in [1] with a complete design procedure and experimental results. In Sec. 4 we review this design concept and present a theoretical quantitative analysis of the tapered structure, which offers encouraging prospects for SWOs.

2. TRAVELING WAVE OSCILLATORS

A basic form of the traveling wave oscillator (TWO) depicted in Fig. 1(a) consists of a distributed amplifier with positive feedback [2] [3]. The TWO directly inherits the major advantage of distributed amplification, the facilitation of oscillation frequencies toward the process-dependent f_T . However, the TWO of Fig. 1(a) suffers from certain disadvantages due to its termination resistors. The forward wave in the gate line and the reverse wave in the drain line are unnecessarily wasted in the termination resistors. Additionally, the termination resistors are constant noise sources which degrade overall phase noise of the oscillator [8].

The rotary traveling wave oscillator (RTWO) of Fig. 1(b) [4] remedies these problems by eliminating the termination resistors and cross-coupling the output and input lines. It also

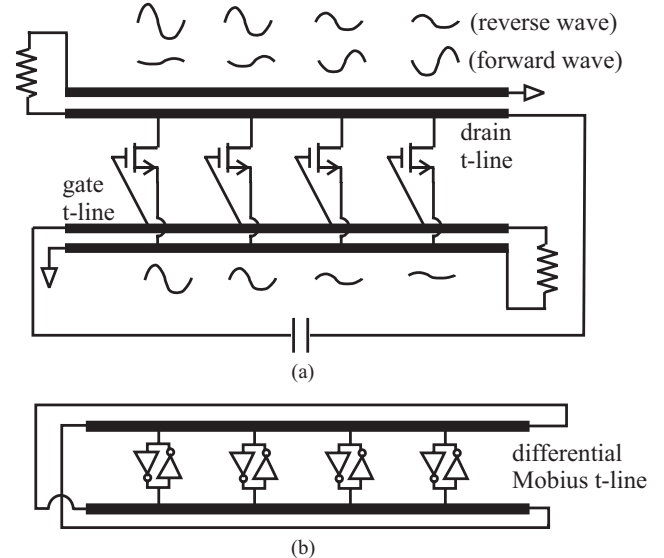


Figure 1: (a) TWO [2] [3]. (b) RTWO [4].

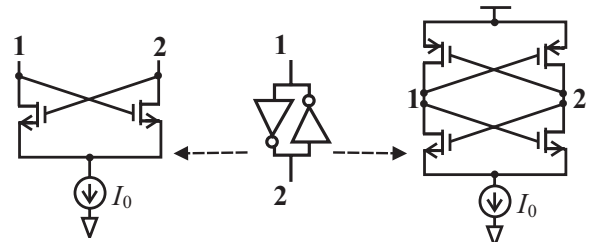


Figure 2: MOSFET-based cross-coupled inverters.

replaces the one-directional amplifiers of the TWO of Fig. 1(a) with cross-coupled inverters, whose symmetry allows use of a single differential transmission line. The resultant differential line takes the form of a Möbius strip where both forward and reverse waves are recycled. The cross-coupled inverters may be realized using cross-coupled NMOS- or CMOS-FETs as shown in Fig. 2.

Standing wave oscillators (SWO) discussed in the next section provide an alternative solution to the shortcomings of the TWO of Fig. 1(a).

3. STANDING WAVE OSCILLATORS

3.1. $\lambda/4$ and $\lambda/2$ SWOs

A $\lambda/4$ SWO depicted in Fig. 3(a) is the most compact SWO configuration [1]. In this SWO a differential transmission line is connected to a pair of cross-coupled inverters at one end and is shorted at the other end. Energy injected as forward waves by the cross-coupled inverters is reflected into reverse waves at the short. In steady state, the forward and reverse waves superpose to form standing waves. While boundary conditions allow standing wave modes at $l = \lambda/4 \times n$ ($n = 1, 3, 5, \dots$), the higher odd modes are insignificant relative to the fundamental mode ($l = \lambda/4$) due to substantial high-frequency loss.

In the fundamental mode the voltage and current amplitudes

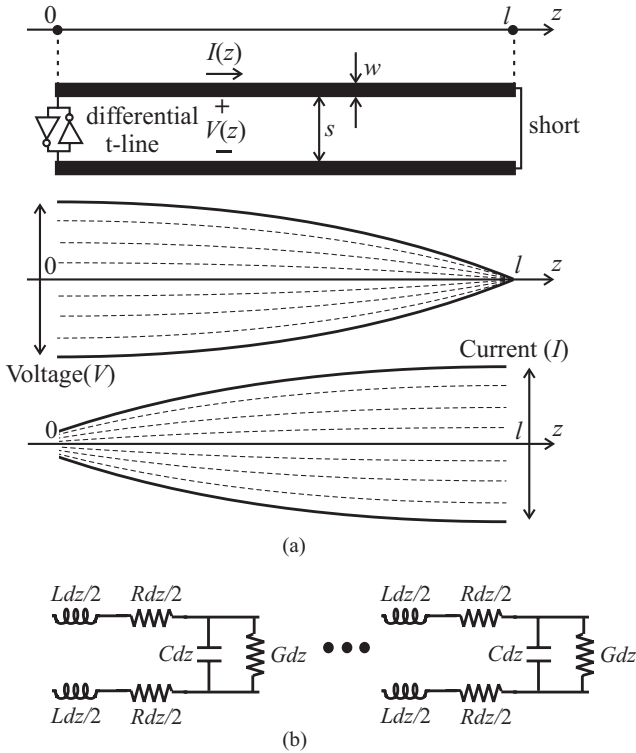


Figure 3: (a) $\lambda/4$ SWO [1] and standing waveforms (fundamental mode). (b) LRCG model for differential transmission lines.

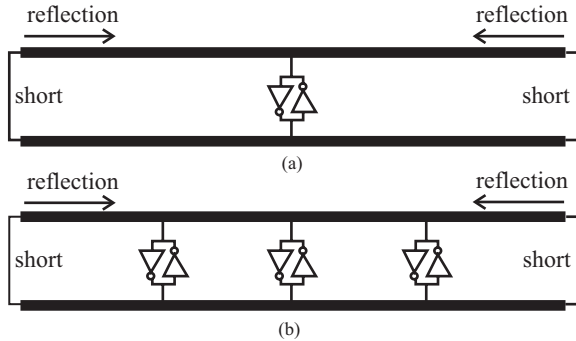


Figure 4: (a) $\lambda/2$ SWO (b) $\lambda/2$ SWO with distributed gain-cells [6]

of the standing wave assume monotonic variations with z as illustrated in Fig. 3(a). At the short end ($z = l$), there is a voltage minimum (zero) and a current maximum. At the other end ($z = 0$) where the cross-coupled inverters are placed, there is a voltage maximum and a current minimum.¹ As will be seen in Sec. 4, this amplitude variation in standing waves makes possible the transmission line tapering technique to lower SWO phase noise.

A variety of other SWOs can be constructed similarly. For instance, Fig. 4(a) shows a $\lambda/2$ SWO, a natural extension of the $\lambda/4$ SWO. The $\lambda/2$ SWO in Fig. 4(a) can be modified as shown in Fig. 4(b), where the line loss is compensated by distributed gain cells [6].

3.2. Circular SWO

All the SWOs presented above rely upon reflective boundaries, but reflection is not a necessary element for standing wave formation [7]. If energy is injected on a ring (close-loop) transmission line as shown in Fig. 5(a), the energy will be split equally and will travel symmetrically along the ring in clockwise and counter-clockwise directions. Thus without any reflection, the

¹The amplitude of this current minimum at $z = 0$ is slightly larger than zero because transistor loading alters the boundary condition such that l is slightly smaller than $\lambda/4$.

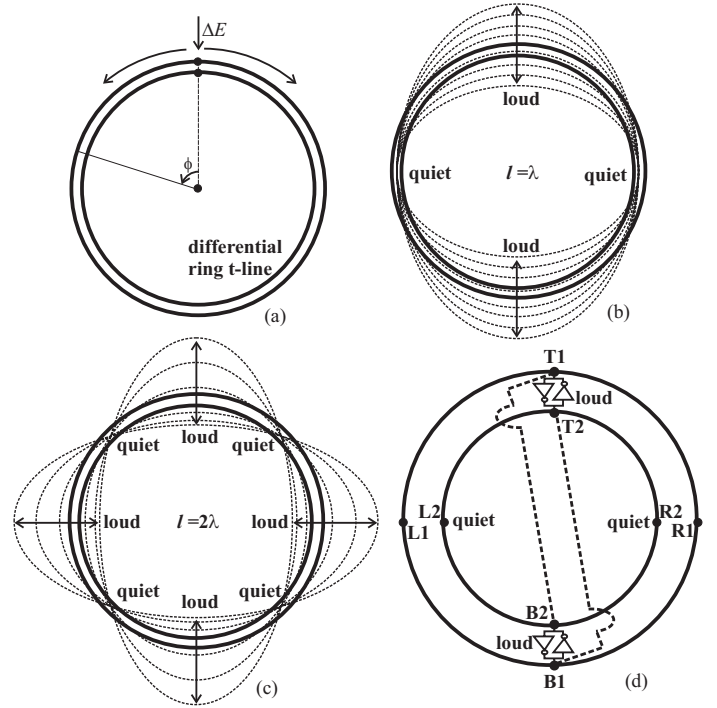


Figure 5: (a) Ring transmission line (b) $l = \lambda$ voltage standing wave (c) $l = 2\lambda$ voltage standing wave (d) Circular standing wave oscillator (CSWO) with even-mode suppression connection (broken lines) [7]

two oppositely traveling waves superpose to form standing waves. The basic selection mechanism determining the various standing wave modes is the *periodic boundary condition* that requires the voltage, $V(\phi)$, at any angle on the ring, to be equal to $V(\phi + 2\pi)$. As a result, the standing wave modes must correspond to $l = n\lambda$ where l is the circumference of the ring, and $n = 1, 2, 3, \dots$. Figures 5(b) and (c) depict voltage waveforms of the fundamental ($n = 1$) and the second ($n = 2$) modes, respectively, each with loud and quiet ports.

The circular standing wave oscillator (CSWO) [7] is constructed by placing cross-coupled inverters at two opposite ports of the ring, T1-T2 and B1-B2, as shown in Fig. 5(d), to compensate loss in the ring. While the CSWO supports all the standing wave modes (practically the first and second modes due to high frequency loss), one may suppress the even-modes vibrations by connecting T1 to B2 and T2 to B1 as shown with broken lines in Fig. 5(d). The connections ensure port T1-T2 and port B1-B2 remain always in opposite phase, which is possible only for odd modes [7]. The major rationale for the even mode suppression is to concentrate more energy in the odd modes (practically, the fundamental mode) for sinusoid generation applications.

3.3. Frequency tuning

The SWO can be made frequency-tunable [9]. Placing a *lumped* varactor on the transmission line and varying the degree of loading allows one to influence the boundary condition, resulting in the frequency tuning. Alternatively, uniform *distribution* of varactors along the transmission line can be used to modify the phase velocity, leading to frequency tuning.

4. STANDING-WAVE ADAPTIVE TAPERING

The previous two sections reviewed various forms of wave-based oscillators and their operations. In this section we review our latest development of standing wave oscillator (SWO) design, the standing-wave adaptive transmission line tapering for lowering SWO phase noise. The original work is reported in [1] and this section is a brief review but with a new theoretical quantitative analysis. The $\lambda/4$ SWO of Fig. 3(a) will be used in this section as a demonstrational vehicle.

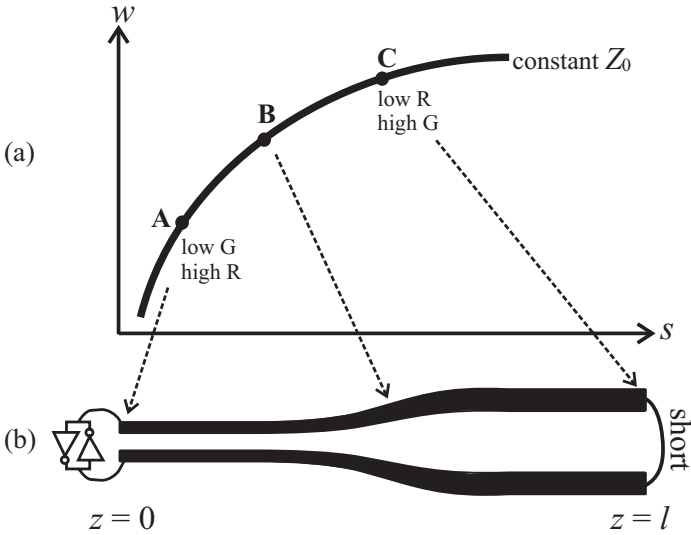


Figure 6: (a) Simulation-based impedance contour in w - s space and R and G variations. (b) $\lambda/4$ SWO using a tapered CPS. [1]

4.1. Basic Concept

For silicon integration, the differential transmission line of Fig. 3(a) can be implemented as an on-chip coplanar stripline (CPS), composed of two metals running in parallel. Figure 3(b) shows the familiar differential $LRCG$ model for the on-chip CPS where L , C , R , and G are inductance, capacitance, series resistance, and shunt conductance per unit length, respectively. Loss within metals due to skin and proximity effects are responsible for the series loss R while interactions with the lossy media outside the metals (underlying substrate and metals) produce the shunt loss G . R couples to current waves as G couples to voltage waves to introduce respective series and shunt losses, directly affecting CPS quality factor, Q , and oscillator phase noise. Low values of R and G are favorable.

Varying metal width, w , and separation, s , of the CPS (w and s are with reference to Fig. 3(a)) is a means of modifying R and G . However, simultaneous minimization of R and G is often impossible; increasing w and s decreases R by mitigating the skin and proximity effects, but increases G by allowing more interaction with the lossy substrate and underlying metals. This trade-off between R and G imposes a major constraint in overall loss minimization when the CPS carries a traveling wave.

When the CPS hosts a standing wave, the R - G tradeoff can be overcome to minimize loss, thanks to the position-dependent standing wave amplitudes. As shown in Fig. 3(a), the $\lambda/4$ SWO has a voltage maximum and current minimum near $z = 0$ and vice versa near $z = l$, so power loss is dominated by shunt conductance G toward $z = 0$ and by series resistance R toward $z = l$. To exploit this property, one should minimize R toward $z = l$ while the unavoidable increase in G is inconsequential due to the negligible voltage amplitude in this vicinity. Likewise toward $z = 0$, one should minimize G while the inevitable increase in R is innocuous due to the locally negligible current amplitude. This position-dependent variation of the loss parameters adapted to the standing wave amplitudes yields a CPS structure that is tapered to reduce loss.

In order to prevent local reflections, the transmission line tapering should be performed while keeping the characteristic impedance, Z_0 , constant throughout the line. This task is facilitated by comprehensive EM simulation data for the CPS, which reveal the dependence of R , G , and Z_0 on a wide range of w and s values [1]. For instance, Fig. 6 shows a simulation-based contour of constant characteristic impedance in w - s space for the CPS in a standard CMOS technology. As one simultaneously moves apart and widens the CPS following this contour, Z_0 remains constant while R decreases and G increases. This R - G tradeoff

was already mentioned. The CPS of our design example, a $\lambda/4$ SWO, can be tapered along this contour as shown in Figs. 6(a) and (b). The voltage maximum and current minimum at $z = 0$ is best suited by a configuration with low G despite high R (point A in 6(a)). At $z = l$ where the current maximum and voltage minimum occurs, a configuration with low R despite high G is employed (point C). Beyond the range from A to C, loss characteristics do not favor tapering. The detailed design procedure is found in [1]. The following subsection quantitatively predicts loss reduction and phase noise improvement due to this line tapering.

4.2. Quantitative Treatment

In this subsection, we will find the tapered transmission line with a constant characteristic impedance, Z_0 , that has minimum loss when hosting a standing wave mode. We will also calculate the uniform transmission line with the same characteristic impedance that has minimum loss when hosting the same standing wave mode. Comparison of the two cases will quantify the loss reduction and Q improvement (and hence phase noise reduction) owing to the tapering.

The total time-averaged loss, P_{diss} , of a single standing wave mode in a general position-dependent transmission line whose horizontal span is l is given by

$$P_{diss} = \int_0^l \left[\frac{1}{2} R(z) I^2(z) + \frac{1}{2} G(z) V^2(z) \right] dz \quad (1)$$

where $I(z)$ and $V(z)$ are current and voltage amplitudes of the standing wave mode at z while $R(z)$ and $G(z)$ are the series and shunt resistances per unit length at z . In the position-dependent transmission line, inductance and capacitance per unit length are not constant so $V(z)$ and $I(z)$ are generally non-sinusoidal and depend on the line structure. Thus (1) is difficult to evaluate in the given form. However, parametrization to the wave's phase, $\theta(z)$, from the physical dimension, z , will greatly simplify the problem. This mapping from z to $\theta(z)$ is useful because in any general transmission line with a constant characteristic impedance, Z_0 , the voltage and current amplitudes for a standing wave mode are *always*² sinusoids of the phase, $\theta(z)$:

$$V(z) = V_0 \cos \theta(z), \quad I(z) = I_0 \sin \theta(z) \quad (2)$$

This is a direct result obtained from the wave equation for the general transmission line [9] where $Z_0 = V_0/I_0$ and $\theta(z)$ is related to z by³

$$\theta(z) = \omega \int_0^z \sqrt{L(z)C(z)} dz \quad (3)$$

Here, ω is the modal frequency, and $L(z)$ and $C(z)$ are inductance and capacitance per unit length at z . With the parametrization to θ , we may rewrite (1) as

$$P_{diss} = \int_0^{\frac{\pi}{2}} \left[\frac{1}{2} (I_0 \sin \theta)^2 R_\theta(\theta) + \frac{1}{2} (V_0 \cos \theta)^2 G_\theta(\theta) \right] d\theta \quad (4)$$

where we have chosen $l = \lambda/4$ and the fundamental $\lambda/4$ mode. Here $R_\theta(\theta) \equiv R(z) \cdot (dz/d\theta)$ and $G_\theta(\theta) \equiv G(z) \cdot (dz/d\theta)$ are series and shunt loss per radian phase shift where $dz/d\theta$ is easily obtained from (3). Now one can easily tackle the loss minimization problem using (4).

The constraint for the minimization of P_{diss} is the previously mentioned R - G tradeoff. While the detailed behavior of the R - G tradeoff is technology dependent, here we require constant product $R_\theta G_\theta$ as an example constraint. The EM simulation used to

²assuming weak loss.

³Note that $\theta(z)$ reduces to the familiar $\omega \sqrt{LC}z = \beta z$ in the uniform line case where β is the phase constant, $2\pi/\lambda$.

produce Fig. 6 reveals that in the technology used for the simulation, the R - G tradeoff along the contour may be approximately described by this constant $R_\theta G_\theta$. Assuming this constraint, we may introduce a constant, $K^2 \equiv R_\theta G_\theta$.

For a uniform line, $R_\theta(\theta) = R_{\theta,0}$ (const.) and $G_\theta(\theta) = G_{\theta,0}$ (const.), and therefore (4) reduces to

$$P_{diss} = \frac{\pi}{8} I_0^2 [R_{\theta,0} + Z_0^2 G_{\theta,0}] \geq \frac{I_0^2 \pi (K Z_0)}{4} \equiv P_{diss,min} \quad (5)$$

where P_{diss} is minimized with respect to $R_{\theta,0}$ (after substituting $G_{\theta,0} = K^2/R_{\theta,0}$) to get $P_{diss,min}$. The minimum occurs when $R_{\theta,0} = K Z_0$ and $G_{\theta,0} = K/Z_0$ (optimum uniform line).

For a tapered (position-dependent) line, the integrand of (4) for a fixed θ is minimized to $(1/2)I_0^2 K Z_0 \sin 2\theta$, which occurs when $R_\theta(\theta) = K Z_0 \cot \theta$ and $G_\theta(\theta) = (K/Z_0) \tan \theta$ (optimum tapered line). The corresponding minimum loss is then

$$P_{diss,min} = \frac{1}{2} I_0^2 K Z_0 \int_0^{\frac{\pi}{2}} \sin 2\theta d\theta = \frac{1}{2} I_0^2 K Z_0 \quad (6)$$

Comparison of (6) to (5) reveals that under the constraint $K^2 = R_\theta G_\theta$ the loss in the optimal tapered line is equal to $2/\pi$ times that in the optimal uniform line when both carrying the same standing wave given by (2).

To calculate the corresponding improvement in Q , we need to consider the energy stored in the transmission lines. The energy stored in a generally position-dependent $\lambda/4$ line with a constant characteristic impedance Z_0 is given by

$$E_{stored} = \int_0^{\frac{\pi}{2}} \left[\frac{1}{4} (I_0 \sin \theta)^2 L_\theta(\theta) + \frac{1}{4} (V_0 \cos \theta)^2 C_\theta(\theta) \right] d\theta \quad (7)$$

when the line hosts the standing wave of (2). Here $L_\theta(\theta) \equiv L(z) \cdot (dz/d\theta)$ and $C_\theta(\theta) \equiv C(z) \cdot (dz/d\theta)$ are inductance and capacitance per radian phase shift. Using $d\theta/dz = \omega \sqrt{L(z)C(z)}$ from (3) and the uniform $Z_0 = \sqrt{L(z)/C(z)}$, we find that $L_\theta(\theta) = Z_0/\omega$ and $C_\theta(\theta) = 1/(\omega Z_0)$, which are independent of θ and solely determined by the modal frequency and the characteristic impedance. Since the tapered line and the uniform line obtained above have the same Z_0 and ω , they also have the same L_θ and C_θ . This, in conjunction with (7), means that the tapered and uniform optimum lines store exactly the same amount of energy. As a result, the loss reduction by a factor of $\pi/2$ due to tapering directly translates to a $\pi/2$ improvement in Q . The familiar Leeson's formula [10] $\mathcal{L}\{\Delta\omega\} = (F/2) \cdot (kT/P_s) \cdot (\omega/(Q\Delta\omega))^2 \sim 1/(P_s Q^2)$ then predicts that phase noise improves by an approximate factor of $(\pi/2)^3 \approx 5.9$ dB as the loss reduction enhances not only Q but also signal power P_s at the oscillator core.

The calculation in this subsection showed a general mathematical method to deal with tapered transmission lines and served to convey a numerical idea on loss reduction, Q enhancement, and phase noise improvement owing to tapering. While capturing the essential concept, the calculation is based on the assumption of constant $R_\theta G_\theta$ which is approximate. The assumption also breaks down eventually as $R_\theta(\theta) = K Z_0 \cot \theta$ and $G_\theta(\theta) = (K/Z_0) \tan \theta$ in the ideal optimum tapered line approach zero and infinity at each end, precluding total optimization in practice. The following subsection briefly presents a real-world design (tapered CPS SWO) example from [1].

4.3. Design Example

Figure 7 shows the die photo for the implemented SWOs with the optimum uniform (left) and tapered (right) CPS from [1]. They were implemented in a $0.18\mu\text{m}$ CMOS technology. The optimum uniform CPS SWO was implemented for the comparison purposes. Calculations using the simulated design parameters

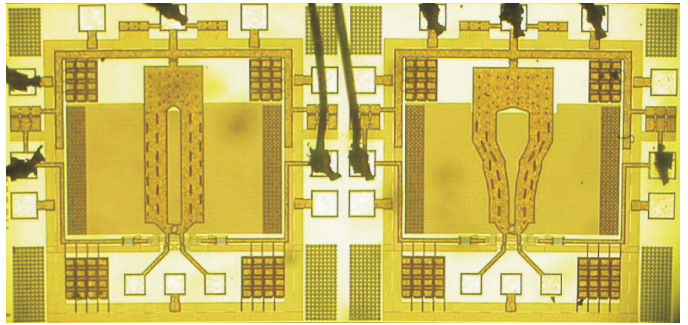


Figure 7: MOS SWO with uniform (left) and tapered (right) CPS.

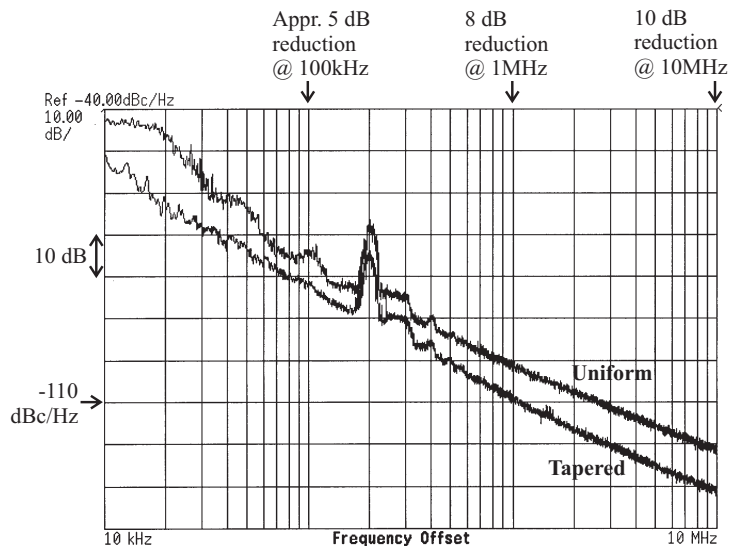


Figure 8: Measured phase noise for the tapered- and uniform-CPS SWOs.

determine that the loss reduction due to tapering is about 1.5, close to the factor, $\pi/2 \approx 1.57$, of the previous subsection. This loss reduction raises the effective CPS Q by 50% to a considerable 59, over the simulated uniform-CPS Q of 39. Figure 8 shows the measured phase noise over 3 decades of offset frequencies for both the tapered-CPS and uniform-CPS SWOs (both SWOs oscillate around 15 GHz). The phase noise improvement due to the tapering is at least 5dB between 10kHz and 1MHz while at greater offset frequencies, the improvement is 8 to 10dB.

5. REFERENCES

- [1] W. Address and D. Ham, "Standing wave oscillators utilizing wave-adaptive tapered transmission lines," To appear in *IEEE VLSI Symposium*, June 2004.
- [2] B. Kleveland *et al.*, "Monolithic CMOS distributed amp. and osc.," *IEEE ISSCC Dig. Tech. Papers*, pp. 70-71, Feb. 1999.
- [3] H. Wu *et al.*, "Silicon-based distributed voltage-controlled oscillators," *IEEE JSSC*, vol. 36, no. 3, Mar. 2001.
- [4] J. Wood *et al.*, "Rotary traveling-wave oscillator arrays: a new clock technology," *IEEE JSSC*, vol. 36, no. 11, Nov. 2001.
- [5] V. Chi, "Salphasic distribution of clock signals for synchronous systems," *IEEE Trans. Comp.*, vol. 43, pp. 597-602, May 1994.
- [6] F. O'Mahony *et al.*, "10GHz clock distribution using coupled standing-wave oscillators," *IEEE ISSCC Dig. Tech. Papers*, pp. 428-429, Feb. 2003.
- [7] D. Ham and W. Address, "A circular standing wave oscillator," *ISSCC Dig. Tech. Papers*, Feb. 2004.
- [8] C. J. White *et al.*, "Phase noise in distributed oscillators," *Electronics Letters*, vol. 38, pp 1453 - 1454, Nov. 2002.
- [9] W. Address, *Theory and Techniques for Standing Wave Oscillators*, B.S. Thesis, Harvard University, 2004.
- [10] D. B. Leeson, "A simple model of feedback oscillator noise spectrum," *Proc. IEEE*, vol. 54, pp. 329-330, Feb. 1966.